NUCL SCI TECH (2019) 30:128
https://doi.org/10.1007/s41365-019-0642-y

Spectrometer of hard X-ray imager payload onboard the ASO-S mission

Yan Zhang[1,2] · Jian-Hua Guo[1] · Zhe Zhang[1] · Deng-Yi Chen[1] · Yi-Ming Hu[1] · Yong-Qiang Zhang[1,2] · Tao Ma[1] · Yong-Yi Huang[1]

Received: 4 January 2019 / Revised: 21 March 2019 / Accepted: 22 March 2019 / Published online: 16 July 2019

Abstract A spaceborne hard X-ray spectrometer, composed of an array of 99 scintillation detectors and associated readout electronics, has been developed for the hard X-ray imager (HXI). The HXI is one of the three payloads onboard the advanced space-based solar observatory (ASO-S), which is scheduled to be launched in early 2022 as the first Chinese solar satellite. $LaBr_3$ scintillators and photomultiplier tubes with a super bialkali cathode are used to achieve an energy resolution better than 20% at 30 keV. Further, a new multi-channel charge-sensitive readout application-specific integrated circuit guarantees high-frequency data acquisition with low power consumption. This paper presents a detailed design of the spectrometer for the engineering model of the HXI and discusses its noise and linearity performance.

Keywords Solar radiation detection · X-ray spectrometer · Hard X-ray imager · ASO-S

This work was supported by the Strategic Priority Program Stage II on Space Science of Chinese Academy of Sciences (No. XDA15320104) and the National Natural Science Foundation of China (Nos. 11703097, 11427803, 11820101002, 11622327, 11773087, U1631116, and 11803093).

✉ Zhe Zhang
zhangzhe@pmo.ac.cn

[1] Key Laboratory of Dark Matter and Space Astronomy, Purple Mountain Observatory, Chinese Academy of Sciences, Nanjing 210034, China

[2] University of Chinese Academy of Sciences, Beijing 100049, China

1 Introduction

The advanced space-based solar observatory (ASO-S) is the first Chinese solar mission within the framework of the strategic priority program stage II (SPPII) on space science of the Chinese Academy of Sciences. Aimed at the 25th solar maximum, the ASO-S is expected to advance our understanding of the solar magnetic field, coronal mass ejections (CMEs), and solar flares. The ASO-S hosts three instruments: a full-disk vector magnetograph, a Lyman-alpha solar telescope, and a hard X-ray imager (HXI), to measure solar magnetic field, CMEs, and solar flares, respectively [1, 2]. The ASO-S is planned to be launched to a 720-km low Earth orbit in early 2022 with a lifetime of four years [3].

The HXI is a spatial X-ray imaging instrument used to determine the location, spectrum, timing, and intensity of accelerated electrons using their bremsstrahlung X-ray emission in the energy range of 30 to 200 keV. The HXI observations could be used to study the acceleration mechanism of electrons and their transportation procedure in the eruptions in the solar atmosphere [3]. The HXI adopts a Fourier-transform imaging technique similar to that used successfully by the hard X-ray telescope on the Yohkoh mission [4], and related to that used on the Reuven Ramaty high-energy solar spectroscopic imager (RHESSI) mission [5] and spectrometer/telescope for imaging X-rays (STIX) on solar orbiter [6].

As a core component of the HXI, a spectrometer composed of scintillation detectors and associated readout electronics has been developed. In this paper, we present the detailed design of the spectrometer for the engineering model of the HXI, after a brief description of the structure of HXI. Comprehensive tests of the spectrometer are

ongoing; nevertheless, we present some preliminary test results that validate our design.

2 Structure of instrument

The schematic view of the HXI is shown in Fig. 1. The HXI consists of three major parts separately mounted on the satellite: the collimator, spectrometer, and electronics control box.

The collimator is based on a titanium alloy framework. A total of 92 pairs of tungsten grid assemblies, the so-called sub-collimators, are arranged at both ends of the framework at a distance of 1200 mm with a solar aspect system. These sub-collimators differ in pitch size from 36 to 800 μm and orientation angles from 9° to 171° to provide different Fourier components of a solar X-ray image. An improved solar aspect system (not shown in Fig. 1) consists of an entrance window of white light, four pieces of frosted glass, and a CMOS camera [7]. It offers accurate pointing knowledge ($\sim$ 2") of the HXI and monitors the distortion of the framework, by measuring the image of the sun from the entrance window and the four frosted glasses.

The spectrometer features an array of 99 detectors, each composed of a $LaBr_3$ scintillator and a photomultiplier tube (PMT). Of these detectors, 92 are aligned with the corresponding sub-collimators for detecting modulated X-ray photons. Three other detectors (without sub-collimators, in the front) are used for recording solar X-ray flux, and the remaining four (with closed apertures) are used to measure the particle background. The front-end electronics (FEEs) and high-voltage distributors are also mounted on the spectrometer.

The electronics control box manages the operations of the HXI, including power supply and transfer of data from the spectrometer and solar aspect system on the collimator to the satellite platform [7]. The main performance requirements of the HXI are summarized in Table 1.

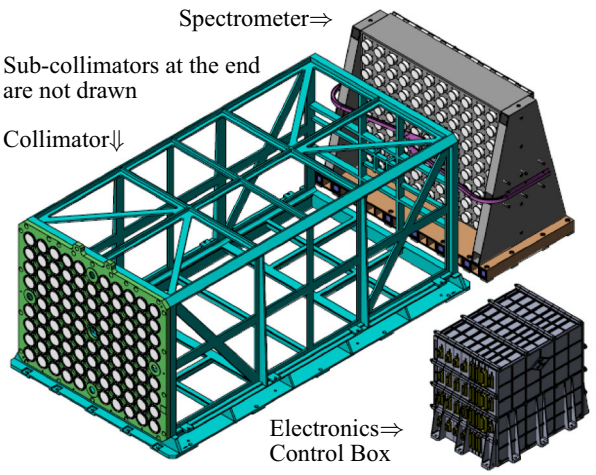

Fig. 1 Schematic view of the HXI payload hardware

3 Design of spectrometer

The spectrometer, which is the focus of this study, measures the solar X-ray spectrum modulated by each sub-collimator in the collimator with both high energy resolution and time resolution. As illustrated in Fig. 2, it contains 99 $LaBr_3$ scintillators arranged in a 9 $\times$ 11 array, with PMTs shielded by permalloy, eight sets of FEEs boards, and high-voltage distribution boards.

When an X-ray photon from the sun hits the scintillator after passing through a pair of sub-collimators, the emitted scintillation light will be collected, transformed, and amplified by the PMT. Subsequently, the PMT signal will be processed by the FEEs, in which a charge measurement application-specific integrated circuit (ASIC) will shape and amplify the signal, and the field-programmable gate array (FPGA) will accumulate it into the spectrum.

3.1 $LaBr_3$ scintillator

The usage of $LaBr_3$ scintillators in high-energy experiments could be traced back to the beginning of this century, and it became an excellent choice for X-ray and γ-ray measurements in a short time [8]. The high light yield and fast decay time of $LaBr_3$ offer both higher energy resolution for X-ray photons at 30 keV and very small probability of signal pile-up during high-intensity flares. An assessment of radiation tolerance shows that there is no measureable degradation of $LaBr_3$ exposed to simulated solar protons with intensity up to 10^{12} protons/cm^2 [9], larger than the expected orbit intensity of $\sim$ 10^{10} protons/cm^2 in a lifetime of four years.

The $LaBr_3$ crystals used in the spectrometer, with a diameter of 25 mm and a height of 25 mm as shown in Fig. 3, were produced by the Beijing Glass Research Institute (BGRI). Owing to the deliquescence of $LaBr_3$, each crystal is packaged in an aluminum shield with a

Table 1 Performance requirements of the HXI

Parameters	Value
Energy range	30–200 keV
Energy resolution (FWHM)	$\leq$ 27% at 30 keV
Finest angular resolution	$\leq$ 6" at 30 keV
Field of view	$\geq$ 40'
Time resolution (statistical limited)	$\leq$ 0.5 s

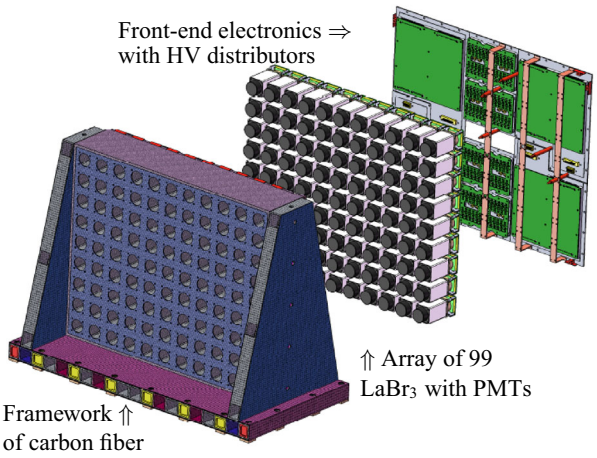

Fig. 2 Architecture of HXI spectrometer

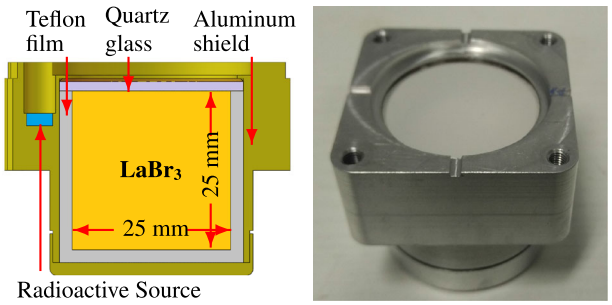

Fig. 3 $LaBr_3$ in X-ray spectrometer: section view and picture

head-on quartz window. Additional Teflon film and optical coupling glue are packed into the shield, to improve the uniformity of light yielded, and to provide sufficient mechanical strength against launch vibrations.

The thickness of the aluminum of the X-ray entrance window of the scintillator must be carefully controlled, as there is no movable attenuator similar to that used in RHESSI and STIX [5, 6]. X-ray attenuation in aluminum with different thicknesses has been calculated with X-ray flux data of a "typical large flare" from RHESSI [10]. The result in Fig. 4 shows that a compromise could be reached in the dilemma of attenuating the flux of X-ray photons below 20 keV without losing too many photons above 30 keV by choosing the thickness of aluminum as 2.5 mm.

An onboard radioactive source is required to calibrate the gain degradation of PMTs and the dependence of FEEs on temperature. Accordingly, ^{133}Ba is chosen for its multiple characteristic X-rays in the energy range 30–383 keV. The intensity is $\sim$ 30 Bq for balancing between the aim of reducing the intrinsic background of the spectrometer, which limits the sensitivity to weak flares, and the requirement of acquiring calibration spectra in $\sim$ 10 min with sufficient statistics.

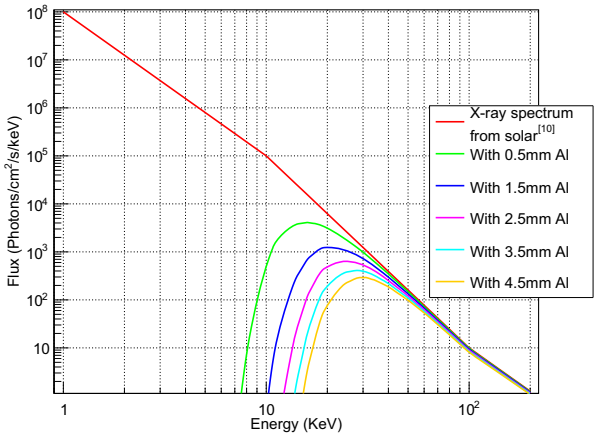

Fig. 4 X-ray attenuation in aluminum (with total cross-section)

3.2 Photomultiplier tube

The PMTs used in the spectrometer are produced by Hamamatsu with a super bialkali cathode to achieve a good energy resolution of X-ray photons at $\sim$ 30 keV. These R1924A-100-01 PMTs, fortified in structure with the criterion adopted by FERMI in a private proposal, could sustain the vibration at launch and the temperature fluctuation in orbit. Figure 5 shows the structure of a PMT installed in a polyimide socket with a permalloy shield to reduce the magnetic field from the earth.

The base circuit of the PMT is limited to an area of 45 $\times$ 45 mm^2, owing to the small installation space in the spectrometer. In the design of the base circuit, a critical issue is to guarantee the linearity and gain stability at high event rate [11]. The circuit is based on Hamamatsu socket E2924-05 [12], with the values of voltage divider resistors and couple capacitors being reduced, as shown in Fig. 6.

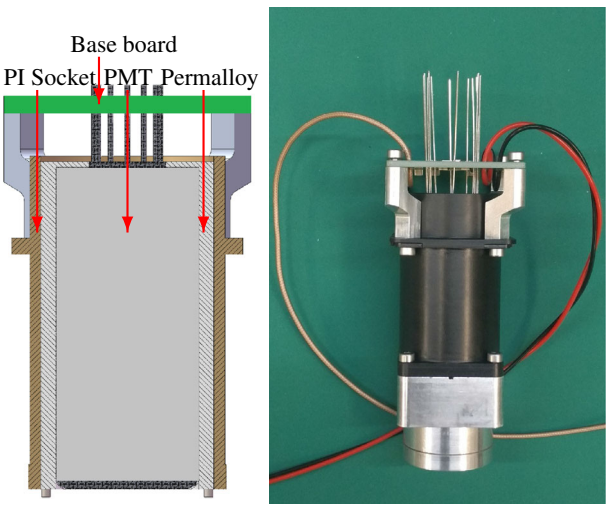

Fig. 5 PMT with socket and base circuits: section view and picture

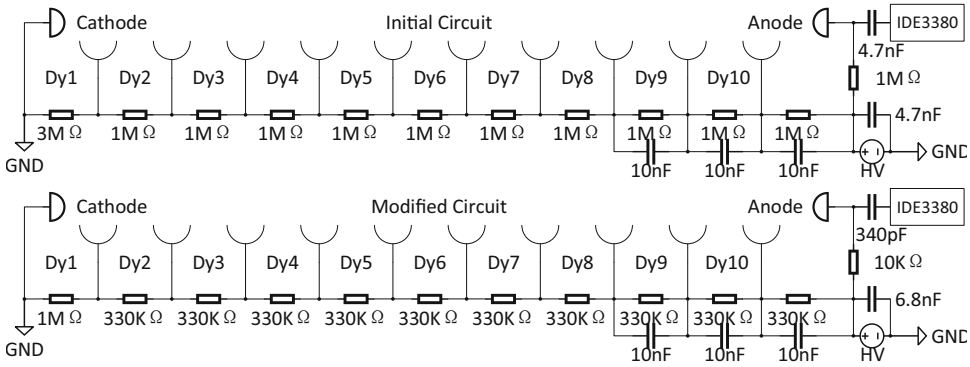

Fig. 6 PMT base circuit: initial (upper) and modified (lower)

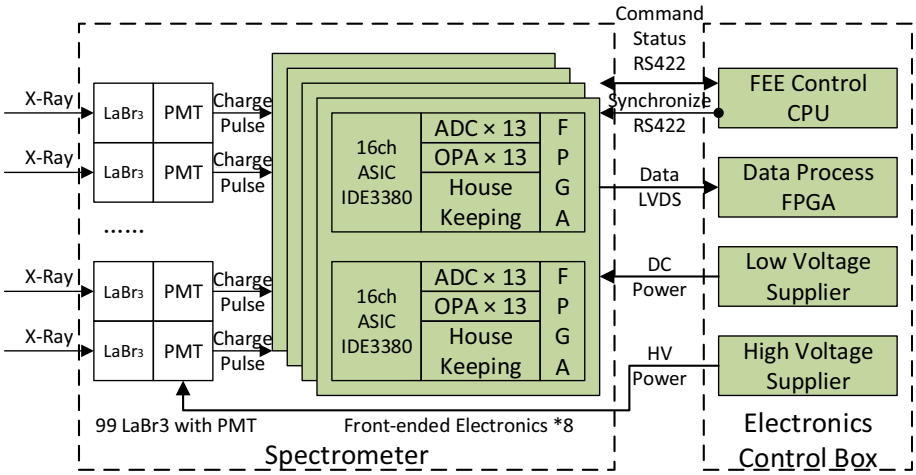

Fig. 7 Architecture of FEEs for the spectrometer

An LED test described in Sect. 4 shows that this circuit provides good linearity and gain stability at an event rate up to 100 kHz.

3.3 Front-end electronics (FEEs)

The architecture of the FEEs is shown in Fig. 7. The signals from all 99 detectors will be connected to eight sets of identical readout circuits, each collecting charge pulses from 12 or 13 PMTs with a 16-channel charge measurement ASIC. The analog outputs of ASIC will be digitalized using analog-to-digital converters (ADCs) under control of the FPGA, and accumulated to form a spectrum. The spectra, together with some other information (such as time code and trigger status), will be packaged by the FPGA and then sent to the electronics control box by an LVDS link with a clock frequency of 25 MHz. The status of the FEEs, and commands from the electronics control box, are both transmitted in a half-duplex RS422-based channel with a user-defined UART protocol. The same protocol is also used in the DArk Matter Particle Explorer (DAMPE) mission [13]. An extra synchronization pulse is sent to all FEEs by the electronics control box simultaneously, to synchronize their beginning and end times. The pulse interval can be adjusted according to the level of solar activity, to reduce data volume during solar quiet periods.

The critical element of the FEEs is the charge measurement ASIC, i.e., IDE3380 from IDEAS, which was originally designed for SiPM, but could also be used for PMTs [14]. This ASIC contains 16 channels, each having a charge-sensitive amplifier, trigger comparator, and CR-RC shaper with track-hold circuit, as shown in Fig. 8. An improved version named IDE3381 is under development

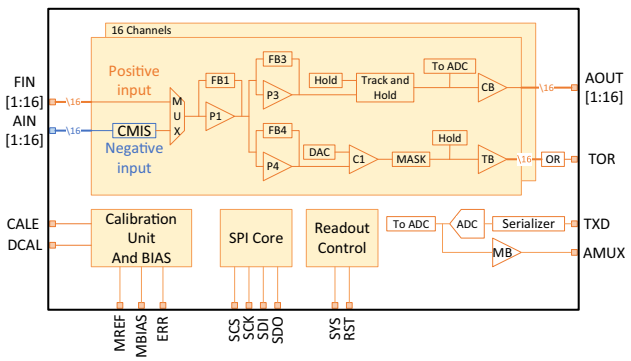

Fig. 8 Block diagram of charge measurement ASIC IDE3380 more details in [14]

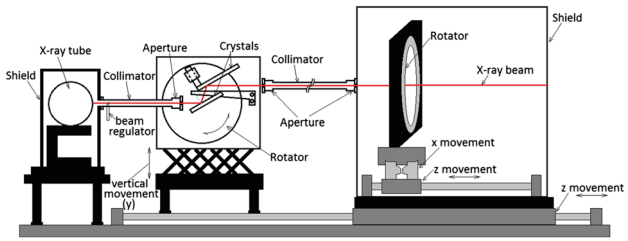

Fig. 9 Schematic diagram of the HXCF [15]

with optimizations in the dynamic range and readout speed, and will be used in the qualification model of the HXI.

There are three types of data produced by FEEs simultaneously: (1) Spectrum data: accumulated from the digitalized output of the ASIC directly and could be used for indirect imaging; (2) Event data: digitalized output with trigger information and could be used for in-orbit trigger threshold calibration; (3) Counting data: obtained from trigger counters in the ASIC, determined by four configurable charge comparators to achieve event counting in different energy ranges, and could be used for flux correction of spectrum and coarse indirect imaging in high-intensity flares. Owing to the limitation of IDE3380, the counting data will only be available in the qualification model of the HXI with the new IDE3381 ASIC.

4 Performance test

4.1 Energy linearity test for $LaBr_3$ with PMT

The energy linearity of the detectors is a critical issue to ensure the reliability of on-orbit observation results. As an absolute necessity, on-ground calibrations of the energy linearity of the detectors have been performed using both X-ray beams and an embedded radiative source. The X-ray beam test has been performed in the hard X-ray calibration facility (HXCF)—an adjustable X-ray beam with a double-crystal monochromator shown in Fig. 9, designed for the Chinese Hard X-ray Modulation Telescope satellite by the Division of Ionizing Radiation Metrology, National Institute of Metrology [15]. This facility could generate X-ray photons covering the energy range 15–100 keV with a monochromaticity better than 0.1%. The $LaBr_3$ detectors are placed in the test platform with a calibrated high-purity germanium detector.

For energy greater than 150 keV, an embedded ^{133}Ba source is used to provide several characteristic lines from 30 to 383 keV. The test result is illustrated in Fig. 10 where error bars are defined by one sigma of a Gaussian distribution, which shows that the integral nonlinearity of $LaBr_3$ with PMT in the energy range 30–383 keV is smaller than 2%.

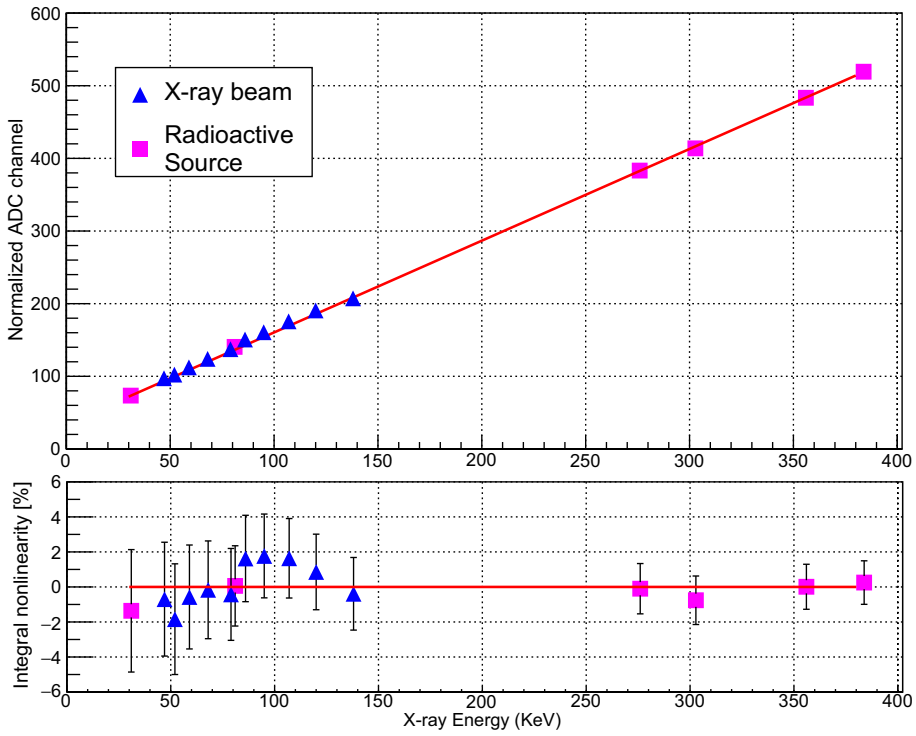

Fig. 10 Energy linearity test results

4.2 Gain stability test for PMT base circuit

Another important milestone in the HXI is to measure the gain stability of PMTs for different event rates. As shown in Fig. 11, an LED test platform driven by a pulse generator has been built in place of the $LaBr_3$ scintillator to simulate the fluorescence induced by X-ray photons. The periodic pulse width has been set to 25 ns, which is same as the decay time of $LaBr_3$. Further, the pulse height has been calibrated by the FEEs, ensuring the light from the LED generates the same amount of charges in the PMT anode as those generated by an X-ray photon with specified energy.

Figure 12 shows the gain stability results obtained with the modified base circuit (Fig. 6) as a function of X-ray event rates. For X-ray photons at 30 keV, the event rate with stable gain could reach up to 100 kHz. Higher event rate will reduce the gain of PMT owing to the saturation in the dynode and anode. With an increase in the energy of X-ray photons, the upper limitation of event rate with stable gain decreases. For a typical solar X-ray spectrum [10], there is a fast exponential decay shape, which indicates that the bottleneck of observation with stable gain in a large flare is the huge flux of X-ray photons in low energy. An attenuation for such huge flux is critical in the design of the spectrometer. In the future, a beam test will be performed to verify the effect of an aluminum shield as the attenuator.

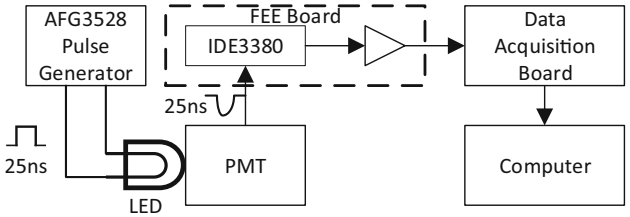

Fig. 11 Block diagram of LED test platform

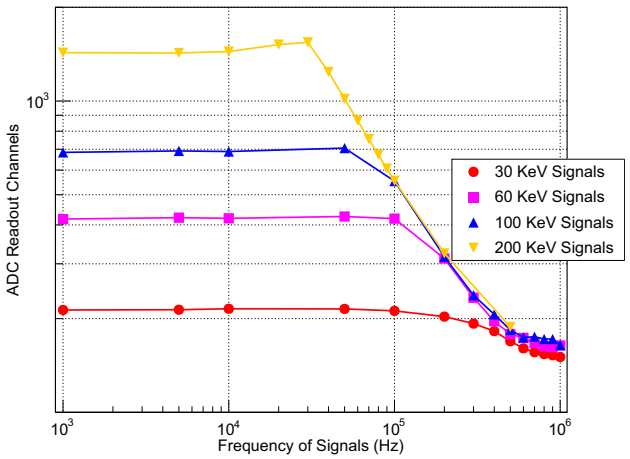

Fig. 12 Results of PMT gain stability test

4.3 Linearity and noise test for ASIC

For monitoring the linearity of ASIC, the same calibration circuit as that used in DAMPE [13] has been added to the FEEs. As shown in Fig. 13, the calibration circuit consists of an analog switch and a coupling capacitor. The step pulse from the analog switch will generate a negative charge on the capacitor similar to the output of the PMT. A

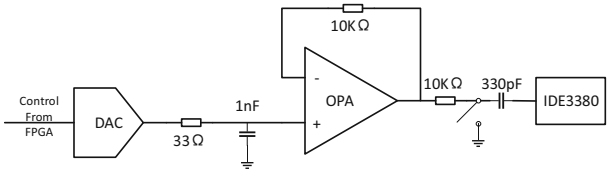

Fig. 13 Block diagram of calibration circuit

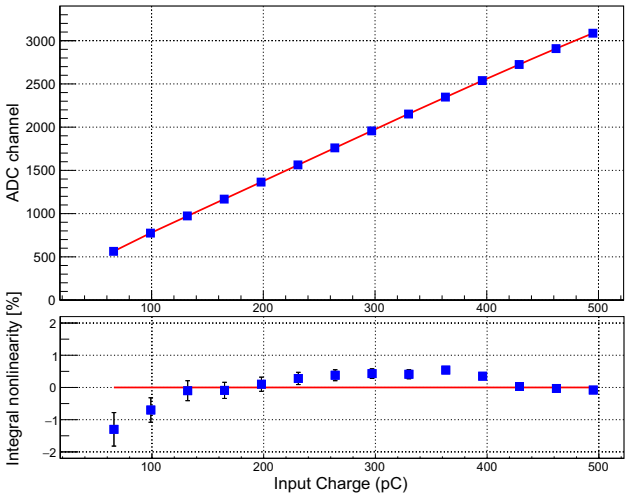

Fig. 14 Linearity performance of ASIC

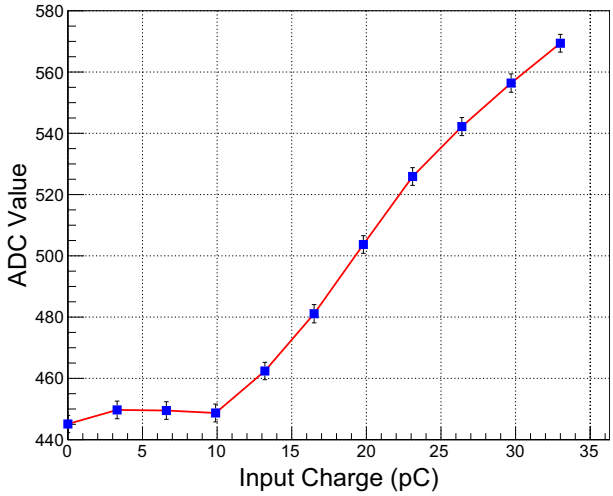

Fig. 15 Noise performance of ASIC

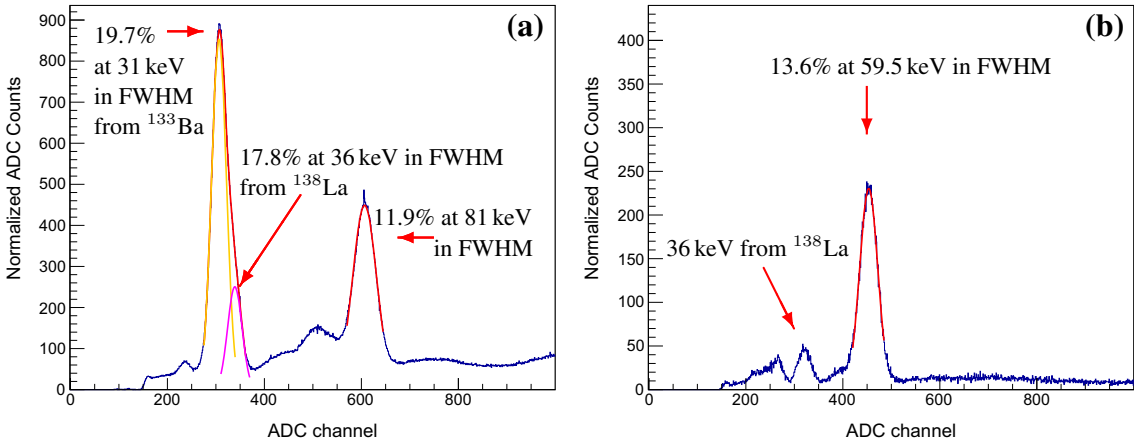

Fig. 16 Spectrum performance (Gaussian fits in red): **a** ^{133}Ba radioactive source, **b** ^{241}Am radioactive source. (Color figure online)

digital-to-analog converter and an amplifier are used to change the voltage of the step pulse for different charge volumes. As shown in Fig. 14, the maximum integral nonlinearity is smaller than 2% with a charge input range of 66–495 pC. The error bars are defined by one sigma of a Gaussian distribution of the ADC channels.

To measure the noise, we feed in a step signal through a 33-pF capacitor and utilize a synchronized external trigger to collect data from the ASIC. The equivalent noise charge (ENC) defined by one sigma of a Gaussian distribution of the ADC data is shown in Fig. 15. With the gain curve measured in Fig. 14, the ENC of ASIC could be estimated as $\sim$ 120 fC, which indicates that the FEEs have no effect on the energy resolution of the spectrometer [16]. Figure 15 also reveals a constant output for signals smaller than $\sim$ 10 pC, which defines the lower limitation of the dynamic range of the FEEs to $\sim$ 10 keV, with an energy-charge conversion factor given by $LaBr_3$ and PMT at $\sim$ 1 pC/keV, smaller than the performance requirement of 30 keV.

4.4 Spectrum performance

The energy resolution of the entire system has been tested using ^{133}Ba and ^{241}Am. As shown in Fig. 16, the full width at half maximum (FWHM) resolution of the spectrometer system is approximately 13.6% at 59.5 keV and 11.9% at 81 keV. The spectrum peak at 300–350 ADC channels is derived from a combination of 31 keV $Cs_{K\alpha}$ X-ray in the decay of ^{133}Ba, and 32 keV $Ba_{K\alpha}$ X-ray with $\sim$ 4 keV Auger electrons in the decay of ^{138}La inside the scintillator. As the proportion of activity between ^{133}Ba and ^{138}La is already known ($\sim$ 8:1), this peak could be fitted with a sum of two Gaussians. The fitting result shows an energy resolution of 19.7% at 31 keV, satisfying the requirement in Table 1.

5 Summary

In this paper, we present the design of the HXI spectrometer for the ASO-S mission, in addition to some tests that validate its performance. The main characteristics of the HXI spectrum, such as energy resolution, energy linearity, and gain stability at high event rate, have been verified in the aforementioned tests. The results from the tests indicate that this design of the spectrometer satisfies the performance requirements of the HXI. Further tests, such as tests on detection efficiency and radiation tolerance, and a beam test with a collimator, will be performed in the qualification model of the HXI.

Acknowledgements The authors would like to thank Prof. Samuel Krucker and Prof. Gordon J. Hurford for their helpful discussions and suggestions. The authors also wish to thank the HXI team who helped make this work possible.

References

1. W.Q. Gan, Q.L. Fan, Space solar physics in China. Chin. J. Space Sci. **38**, 662–664 (2018). https://doi.org/10.11728/cjss2018.05.662
2. W.Q. Gan, Y. Huang, Y.H. Yan, The past and future of space solar observations. Sci. China Ser. G **42**, 1274 (2012). https://doi.org/10.1360/132012-658
3. W.Q. Gan, Y.Y. Deng, H. Li et al., ASO-S: advanced space based solar observatory. Proc. SPIE **9604**, 96040T (2015). https://doi.org/10.1117/12.2189062
4. T. Kosugi, K. Makishima, T. Murakami et al., The hard X-ray telescope (HXT) for the SOLAR-A mission. Sol. Phys. **136**, 17 (1991). https://doi.org/10.1007/BF00151693
5. G.J. Hurford et al., The RHESSI imaging concept, in *The Reuven Ramaty High-Energy Solar Spectroscopic Imager (RHESSI)*, ed. by R.P. Lin, A.O. Benz (Springer, New York, 2003). https://doi.org/10.1007/978-94-017-3452-3_3
6. S. Krucker, M. Bednarzik, O. Grimm et al., The spectrometer/telescope for imaging X-rays on solar orbiter: flight design,

challenges and trade-offs. Nucl. Instrum. Methods Phys. Res. A **824**, 626–629 (2016). https://doi.org/10.1016/j.nima.2015.08.045
7. S. Wang, J.H. Guo, Y. Zhang et al., High-resolution pixelated CdZnTe detector prototype system for solar hard X-ray imager. Nucl. Sci. Tech. **30**, 42 (2019). https://doi.org/10.1007/s41365-019-0571-9
8. E.V.D. Van Loef, P. Dorenbos, C.W.E. Van Eijk et al., Scintillation properties of LaBr 3:Ce3+ crystals: fast, efficient and high-energy-resolution scintillators. Nucl. Instrum. Methods Phys. Res. A **486**, 254–258 (2002). https://doi.org/10.1016/S0168-9002(02)00712-X
9. A. Owens, A.J.J. Bos, S. Brandenburg et al., Assessment of the radiation tolerance of LaBr 3: Ce scintillators to solar proton events. Nucl. Instrum. Methods Phys. Res. A **572**(2), 785–793 (2007). https://doi.org/10.1016/j.nima.2006.12.008
10. R.P. Lin et al., The Reuven Ramaty high-energy solar spectroscopic imager, in *The Reuven Ramaty High-Energy Solar Spectroscopic Imager (RHESSI)*, ed. by R.P. Lin, A.O. Benz (Springer, New York, 2003). https://doi.org/10.1007/978-94-017-3452-3_1
11. Z.Y. Zhang, Y.L. Zhang, J.N. Dong et al., Design of a high dynamic range photomultiplier base board for the BGO ECAL of DAMPE. Nucl. Instrum. Methods Phys. Res. A **780**, 21–26 (2015). https://doi.org/10.1016/j.nima.2015.01.036
12. Hamamatsu, Photomultiplier tubes basics and applications. PMT_handbook_v3aE.pdf
13. C.Q. Feng, D.L. Zhang, J.B. Zhang et al., The design of the readout electronics for the BGO calorimeter of DAMPE mission. IEEE Trans. Nucl. Sci. **62**, 3117–3125 (2015). https://doi.org/10.1109/TNS.2015.2479091
14. D. Meier, J. Ackermann, A. Olsen et al., in *Proceedings of the ESA AMICSA & DSP, 6th International Workshop*. SIPHRA 16-channel silicon photomultiplier readout ASIC (2016)
15. X. Zhou, X.Q. Li, Y.N. Xie et al., Introduction to a calibration facility for hard X-ray detectors. Exp. Astron. **38**, 433–441 (2014). https://doi.org/10.1007/s10686-014-9393-2
16. M.S. Alekhin, J.T.M. De Haas, I.V. Khodyuk et al., Improvement of γ-ray energy resolution of $LaBr_3$: Ce^{3+} scintillation detectors by Sr^{2+} and Ca^{2+} co-doping. Appl. Phys. Lett. **102**, 161915 (2013). https://doi.org/10.1063/1.4803440